

# Capacity Analysis of ORS-assisted Free Space Optical Communication Systems

**B . Tech. Project**

*Submitted in partial fulfillment of the requirements*

*of the degree of*

**Bachelor of Technology**

in

**Electrical Engineering**

By

**Deepak Jaladi**

(Roll No: 210002039 )

Under the guidance of

**Dr. Swaminathan Ramabadran**



**Department of Electrical Engineering**

**Indian Institute of Technology Indore**

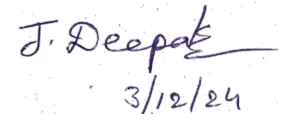
**Dec. 2024**

# Declaration

I hereby declare that the project entitled “**Capacity Analysis of ORS-assisted Free Space Optical Communication Systems**” submitted in partial fulfilment for the award of the degree of Bachelor of Technology in ‘**Electrical Engineering**’ completed under the supervision of **Dr. Swaminathan Ramabadran, Associate Professor, Discipline of Electrical Engineering, IIT Indore** is an authentic work.

Further, I declare that I have not submitted this work for the award of any other degree elsewhere.

I declare that this written submission represents my ideas in my own words and where other’s ideas or words have been included, I have adequately cited and referenced the original sources. I also declare that I have adhered to all principles of academic honesty and integrity and have not misinterpreted or fabricated or falsified any idea/data/fact/source in my submission. I understand that any violation of the above will be cause for disciplinary action by the institute and can also evoke penal action from the sources which have thus not been properly cited or from whom proper permission has not been taken when needed.



Deepak Jaladi

NAME OF THE STUDENT

Date: 03/12/2024

Place: Indore

# Preface

This report on “**Capacity Analysis of ORS-assisted Free Space Optical Communication Systems**” is prepared under the guidance of Dr. Swaminathan Ramabadran.

In this report, I have analyzed the ergodic capacity performance of a multi-hop ORS-assisted FSO system. In particular, the ORS-assisted multihop FSO system is analyzed under decode-and-forward relaying. Finally, I have obtained the results using the derived analytical expression and validated it using Monte-Carlo simulation. I have tried my best to explain the content concisely yet profoundly.

**DEEPAK JALADI**

B. Tech. IV year

Department of Electrical Engineering

## B. Tech. Project Approval Certificate

This is to certify that the dissertation titled “**Capacity Analysis of ORS-assisted Free Space Optical Communication Systems**” submitted by **Deepak Jaladi**, (Roll No.210002039) is approved for the award of degree of **Bachelor of Technology** in **Electrical Engineering**.



BTP Supervisor(s): Swaminathan R

Date: 03/12/2024

Designation: Associate Professor

## Acknowledgements

I would like to express my deepest gratitude to my project guide, Dr. Swaminathan Ramabadran, for his invaluable guidance, unwavering support, and immense patience throughout the course of this project. His ability to simplify complex concepts and his encouragement to explore innovative ideas have been instrumental in shaping the direction and quality of my work. I am truly thankful for his constant motivation and the time he devoted to helping me overcome challenges during this journey.

I am also profoundly grateful to Mr. Prashant Sharma for his insightful advice, technical expertise, and constructive feedback, which greatly enriched my understanding of the subject and enhanced the outcomes of this project. His valuable suggestions and encouragement were pivotal in addressing key challenges during this research.

Lastly, I would like to thank my parents and friends, whose unwavering support, encouragement, and belief in my abilities have been a constant source of inspiration. Their understanding and emotional backing gave me the strength to persevere through the demanding phases of this project. I am truly indebted to all of them for standing by me and contributing to the successful completion of this work.

## Abstract

This study examines the ergodic capacity of a multihop ORS-assisted free-space optical (FSO) communication system using decode-and-forward relaying. The system model accounts for atmospheric turbulence using Gamma-Gamma, Malaga, and doubly inverted Gamma-Gamma distributions. The analysis considers the effect of ORS on channel quality through intelligent beam redirection and optimization. Closed-form expressions for ergodic capacity are derived, considering key system parameters like hop number, relay positions, and ORS elements. Numerical results show a significant improvement in ergodic capacity, especially under adverse turbulence conditions. The study highlights the potential of ORS technology to enhance FSO systems' performance, making them more reliable and efficient for high-capacity communication in challenging atmospheric scenarios. The results are validated through Monte-Carlo simulations, demonstrating their accuracy and practical applicability for the design and optimization of next-generation optical wireless communication systems.

***Keywords*** – Ergodic Capacity, ORS, FSO, decode-and-forward, Gamma–Gamma, Málaga, Doubly inverted Gamma-Gamma.

# Contents

|   |             |
|---|-------------|
| <b>List of Figures</b>  | <b>viii</b> |
| <b>List of Tables</b>   | <b>ix</b>   |
| <b>1 Introduction</b>   | <b>1</b>    |
| 1.1 Background . . . . .  | 1           |
| 1.2 Literature Survey . . . . .   | 3           |
| 1.3 Motivations and Contributions . . . . .                                     | 4           |
| 1.4 Organization of the Report . . . . .  | 4           |
| <b>2 System Model of ORS-assisted FSO System with DF relaying</b>               | <b>6</b>    |
| 2.1 System and channel model . . . . .  | 6           |
| 2.1.1 Atmospheric turbulence fading model . . . . .                             | 7           |
| 2.1.2 Pointing error fading model . . . . .                                     | 8           |
| 2.1.3 Fog fading model . . . . .  | 9           |
| 2.2 Combined channel model . . . . .  | 9           |
| 2.2.1 Gamma-Gamma distribution . . . . .  | 9           |
| 2.2.2 Málaga Distribution . . . . .   | 10          |
| 2.2.3 IGGG Distribution . . . . .   | 12          |
| <b>3 Ergodic Capacity analysis of the system using Gamma-Gamma distribution</b> | <b>14</b>   |
| <b>4 Ergodic Capacity analysis of the system using Málaga distribution</b>      | <b>16</b>   |
| <b>5 Ergodic Capacity analysis of the system using IGGG distribution</b>        | <b>18</b>   |
| <b>6 Numerical Results and Discussions</b>                                      | <b>20</b>   |
| <b>7 Conclusions and Future Work</b>  | <b>26</b>   |
| 7.1 Conclusion . . . . .  | 26          |

|                                    |           |
|------------------------------------|-----------|
| 7.2 Future scope of work . . . . . | 26        |
| <b>References</b>                  | <b>27</b> |



# List of Figures

|     |   |    |
|-----|---|----|
| 2.1 | IRS-assisted multihop FSO system . . . . .  | 6  |
| 6.1 | Flowchart of Monte-Carlo simulations for calculating ergodic capacity . . .                     | 21 |
| 6.2 | Ergodic capacity performance for N hops . . . . .   | 21 |
| 6.3 | Ergodic capacity performance for different values of pointing error . . . . .                   | 22 |
| 6.4 | Ergodic capacity performance for different foggy weather conditions . . . .                     | 22 |
| 6.5 | Ergodic capacity performance for different link distances . . . . .                             | 23 |
| 6.6 | Ergodic capacity performance for different refractive index structure pa-<br>rameters . . . . . | 24 |
| 6.7 | Comparison of ergodic capacity between systems with and without ORS .                           | 24 |
| 6.8 | Comparision between Gamma–Gamma, Málaga and IGGG distributions .                                | 25 |

# List of Tables

|     |  |    |
|-----|--|----|
| 1.1 | Literature review . . . . .                      | 3  |
| 2.1 | List of notations . . . . .                      | 13 |
| 3.1 | List of notations for ergodic capacity . . . . . | 15 |
| 6.1 | Simulation parameters . . . . .                  | 20 |

# Chapter 1

## Introduction

### 1.1 Background

Free-space-optics (FSO) communication is a wireless communication technology that uses light signals, typically in the infrared or visible spectrum, to transmit data through free space. It involves lasers or LEDs at the transmitter to send optical beams carrying information, which are then detected and converted back into electrical signals by a photodetector at the receiver. FSO operates without physical cables or infrastructure, making it highly adaptable for line-of-sight communications, such as inter-building communication, satellite links, and last-mile connectivity in urban environments. Its high bandwidth and immunity to electromagnetic interference make it a promising alternative to traditional radio frequency (RF) communication.

FSO communication offers several advantages over RF communication. Firstly, FSO provides significantly higher data rates due to the smaller wavelength of optical signals, enabling a greater capacity to transfer information. Secondly, unlike RF, which often requires regulatory permissions and incurs spectrum costs, it operates in an unlicensed spectrum. Additionally, FSO systems are highly secure because the narrow beam divergence reduces the risk of signal interception. Light signals also eliminate RF interference issues, making FSO signal suitable for dense urban settings or electromagnetic-sensitive environments, such as hospitals and airports. However, FSO systems are susceptible to atmospheric effects such as rain, fog, and turbulence, which can degrade signal quality and limit its range.

Intelligent Reflecting Surfaces (IRS) are a transformative technology for wireless communication systems, enhancing signal propagation by manipulating the wireless environment. An IRS includes many passive, programmable reflective elements that can change

the phase, amplitude, or polarization of signals to enhance channel's quality and reliability. They are used to avoid obstacles, decrease path losses, and increase energy efficiency, especially in line-of-sight blockages.

IRS holds several advantages over traditional communication approaches. It is energy-efficient as it relies on passive components that consume minimal or no power compared to active relays or antennas. Additionally, IRS improves spectral efficiency by enhancing signal strength in desired directions, reducing interference, and providing flexibility in network design. The technology also supports secure communication by directing signals toward specific users, mitigating eavesdropping risks. Moreover, IRS is scalable and cost-effective, as its deployment does not require complex circuitry or significant maintenance.

An IRS can be adapted for free-space optical communication, where it becomes an optical reflecting surface (ORS). An ORS leverages the principles of the IRS but is specifically designed to work with optical signals. ORS reflects and modulates light beams to optimize their trajectory toward the receiver, overcoming obstacles such as buildings or atmospheric distortions. By implementing ORS, FSO communication can achieve improved LoS connectivity and resilience against physical barriers.

The advantages of ORS include enhanced reliability and coverage in FSO systems by mitigating LoS blockages and atmospheric disturbances. ORS systems are passive and require little or negligible external power for operations, making them highly energy-efficient. They also support multi-user environments by directing light beams dynamically based on user position and maximize resource utilization. Furthermore, ORS enables cost-effective deployment, as it does not require active amplification or signal processing components which reduce operational complexity.

Multihop FSO communications involves multiple intermediate nodes between the transmitter and receiver. These nodes can be active relays or passive reflecting surfaces, such as ORS. The multihop approach extends the communication range and enhances system performance by dividing the long optical path into smaller, manageable segments. Multihop FSO systems also improve signal reliability in scenarios with significant atmospheric attenuation or obstructions.

Decode-and-Forward (DF) and Amplify-and-Forward (AF) are two techniques for relaying, used in multihop systems. AF relaying technique amplifies received signals, including noise, and forwards them to the next hop. It's simple and requires minimal processing, but its main drawback is noise propagation, which can degrade the signal-to-noise ratio.

On the other hand, DF really involves decoding the received signal, removing the noise,

and then re-encoding and transmitting a clean version to the next hop. DF provides a significant performance advantage over AF because it eliminates noise accumulation over multiple hops, improving the system's reliability and SNR. However, DF is more complex and energy-intensive as it requires signal processing and re-transmission at each relay. DF is particularly beneficial in FSO systems, where maintaining signal integrity over long distances is critical.

The multihop approach, combined with DF relaying, is highly advantageous for FSO systems. It enables reliable long-distance communication by mitigating the impact of attenuation and ensuring robust signal quality across hops. Multihop systems also allow for flexible deployment in challenging environments, such as urban areas or mountainous terrains, by strategically placing intermediate relays or ORS at optimal locations. By leveraging DF relaying, FSO systems can achieve higher data rates and improved resilience against noise, interference, and atmospheric disturbances. As FSO communication continues to evolve, the integration of technologies such as ORS and advanced relaying techniques promises to unlock new possibilities for high-speed, reliable, and energy-efficient wireless communication networks.

## 1.2 Literature Survey

Table 1.1: Literature review

| Reference  | Type of system            | Link distribution                 | Metrics         |
|------------|---------------------------|-----------------------------------|-----------------|
| [1]        | Dual-hop (DH) FSO         | Gamma–Gamma                       | ABER, OP and EC |
| [2]        | DH FSO/RF                 | FSO–Gamma–Gamma,<br>RF–Nakagami–m | ABER, OP and EC |
| [3]        | Multihop FSO              | Gamma–Gamma                       | OP              |
| [4]        | DH IRS–assisted FSO/RF    | FSO–Gamma–Gamma,<br>RF–Rayleigh   | ABER, OP        |
| [5]        | Multihop IRS–assisted FSO | Gamma–Gamma                       | ABER, OP        |
| This model | Multihop ORS–assisted FSO | Gamma–Gamma,<br>Málaga, IGGG      | EC              |

## 1.3 Motivations and Contributions

The motivations behind the work are summarized as follows:

- The existing literature has analyzed Multihop FSO without ORS.
- The Multihop scenario improves the coverage and this sort of model is proposed keeping in mind the dense urban environment.
- Using ORS in each hop helps to enable a virtual line-of-sight (LoS) between the transmitter and detector which improves the system's performance.

The contributions of the work are summarized as follows:

- We proposed a Multihop ORS-assisted FSO system with N hops with an ORS in each hop.
- The end-to-end probability distribution function (PDF) of instantaneous SNR for each hop is derived using direct detection (DD) technique.
- Closed-form expressions for ergodic capacity have been derived considering factors such as atmospheric turbulence, pointing errors, and fog. Atmospheric turbulence fading in FSO is modelled using Gamma-Gamma, Málaga, and doubly inverted Gamma-Gamma (IGGG) distributions, with ergodic capacity expressions obtained for each model.
- We compared the performance between Multihop ORS-assisted FSO and Multihop FSO without ORS.
- Monte-Carlo simulations were utilized to verify the accuracy of our derived expressions.

## 1.4 Organization of the Report

The rest of this report is organized as follows: Chapter 2 presents the system model, offering a comprehensive description of the multihop ORS-assisted FSO communication framework, which serves as the foundation for the subsequent analysis. Chapters 3, 4, and 5 are dedicated to deriving the ergodic capacity of the proposed system under varying turbulence conditions, modelled using the Gamma-Gamma, Málaga, and IGGG distributions, respectively. These chapters delve into the mathematical formulations and provide

insights into the system's performance under different fading scenarios. Chapter 6 presents numerical results and discusses the implications of the derived expressions, supported by simulations and graphical analysis. Finally, Chapter 7 concludes the report by summarizing the key findings and proposing directions for future research in enhancing the performance of FSO communication systems.

# Chapter 2

## System Model of ORS-assisted FSO

### System with DF relaying

#### 2.1 System and channel model

In this chapter, we have discuss the system and channel modeling for the multi-hop ORS-assisted FSO communication system with the DF relaying technique. For the proposed system model, we have derived the closed-form expression for the probability distribution function (PDF) for different statistical models of atmospheric turbulence like Gamma-Gamma, Málaga, and IGGG distributions. Fig. 2.1 illustrates the system model of a

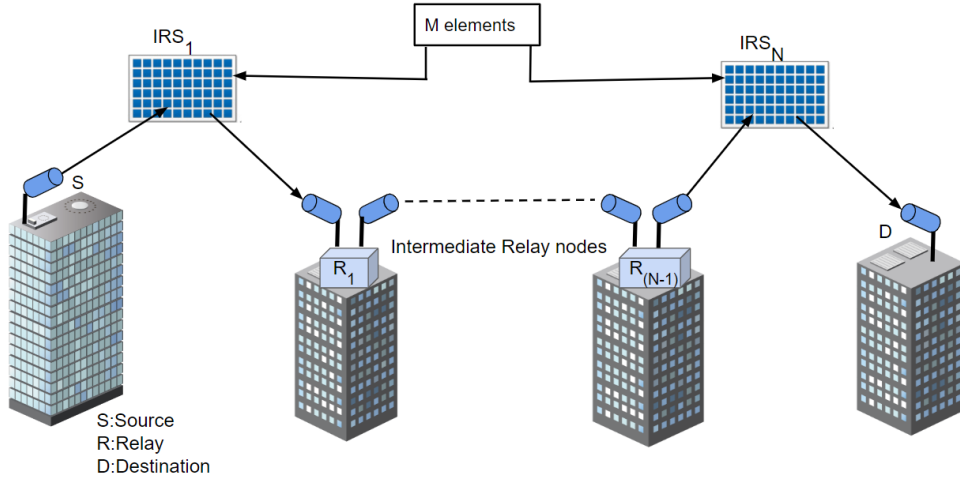


Figure 2.1: IRS-assisted multihop FSO system

multihop IRS-assisted FSO system employing DF relaying with  $N$  hops and  $M$  reflecting elements for each IRS. The model considers  $N$  relay ( $R$ ) nodes between the source ( $S$ ) and destination ( $D$ ). The link distance between each  $R$  is assumed to be equal (i.e.,  $L^{(1)}=L^{(2)}=\dots=L^{(p)}=L$ , where  $p = 1..N$ ), and the distances from the transmitter ( $Tx$ ) to



the IRS and from the IRS to the receiver ( $Rx$ ) are also assumed to be equal (i.e.,  $L_1 = L_2$ ). We are assuming  $M = 1$  for each IRS which converts the IRS into ORS. So, the overall channel coefficient of the  $p^{th}$  hop,  $Z_p$  can be written as  $Z_p = h_1^{(p)} h_2^{(p)}$ , where  $h_1^{(p)}$  is the channel coefficient from Tx to ORS and  $h_2^{(p)}$  is the channel coefficient from ORS to Rx of any  $p^{th}$  hop and the received FSO signal at the photodetector of any  $p^{th}$  hop is given as [5]

$$y_p = Z_p x_p + n_p \quad (2.1)$$

where  $x_p$  is the message signal transmitted from Tx and  $n_p$  is the AWGN with zero-mean and variance  $\sigma_{op}^2$  for any  $p^{th}$  hop. We assume that the transmitted message signal will encounter signal fading due to atmospheric turbulence, pointing errors, and foggy weather conditions, which are statistically modelled below.

### 2.1.1 Atmospheric turbulence fading model

#### Gamma-Gamma Distribution

The PDF of atmospheric turbulence from Tx to ORS of any  $p^{th}$  hop,  $f_{h_a}^{(p)}$  is given as [5]

$$f_{h_a}^{(p)}(x) = \frac{2(\alpha^{(p)}\beta^{(p)})^{\frac{\alpha^{(p)}+\beta^{(p)}}{2}}}{\Gamma(\alpha^{(p)})\Gamma(\beta^{(p)})} x^{\frac{\alpha^{(p)}+\beta^{(p)}}{2}-1} K_{\alpha^{(p)}-\beta^{(p)}}(2\sqrt{\alpha^{(p)}\beta^{(p)}}x) \quad (2.2)$$

where  $\alpha^{(p)}$  and  $\beta^{(p)}$  are the large and small scale scattering parameters and  $K_d(\cdot)$  is the modified vessel function of second kind and  $d^{th}$  order,  $\Gamma(\cdot)$  is the Gamma function. The expressions for  $\alpha^{(p)}$  and  $\beta^{(p)}$  are given as

$$\begin{aligned} \alpha^{(p)} &= [\exp(0.49(\Omega^{(p)})^2(1 + 0.56(\Omega^{(p)})^{12/5})^{-7/6} - 1)]^{-1}, \\ \beta^{(p)} &= [\exp(0.51(\Omega^{(p)})^2(1 + 0.69(\Omega^{(p)})^{12/5})^{-5/6} - 1)]^{-1}, \end{aligned} \quad (2.3)$$

where  $(\Omega^{(p)})^2 = 0.5C_n^2 k^{7/6} (L_1^{(p)})^{(11/6)}$  is Rytov variance,  $C_n^2$  is refractive index parameter,  $k$  is optical wavenumber and  $L_1^{(p)}$  is the link distance between Tx and ORS.

#### Málaga Distribution

The PDF of atmospheric turbulence from Tx to ORS of any  $p^{th}$  hop,  $f_{h_a}^{(p)}$  is given as [6]

$$f_{h_a}^{(p)}(x) = A_M \sum_{d^{(p)}=1}^{\beta^{(p)}} a_d x^{\frac{\alpha^{(p)}+d^{(p)}}{2}-1} K_{\alpha^{(p)}-\beta^{(p)}} \left( 2\sqrt{\frac{\alpha^{(p)}\beta^{(p)}x}{y^{(p)}\beta^{(p)} + \Omega'^{(p)}}} \right) \quad (2.4)$$

The expressions for  $A_M$  and  $a_d$  are given as

$$A_M^{(p)} = \frac{2\alpha^{(p)\alpha^{(p)}/2}}{y^{(p)1+\alpha^{(p)}/2}\Gamma(\alpha^{(p)})} \left( \frac{y^{(p)}\beta^{(p)}}{y^{(p)}\beta^{(p)} + \Omega^{(p)}} \right)^{\beta^{(p)}+\alpha^{(p)}/2} \quad (2.5)$$

$$a_d^{(p)} = \left( \frac{\beta^{(p)} - 1}{d^{(p)} - 1} \right) \frac{(y^{(p)}\beta^{(p)} + \Omega^{(p)})^{1-d^{(p)}/2}}{(d^{(p)} - 1)!} \left( \frac{\Omega^{(p)}}{y^{(p)}} \right)^{d^{(p)}-1} \left( \frac{\alpha^{(p)}}{\beta^{(p)}} \right)^{d^{(p)}/2} \quad (2.6)$$

where  $\Omega^{(p)}$  and  $y^{(p)}$  are parameters related to the power of scattering components. [6]

### IGGG distribution

The PDF of atmospheric turbulence from Tx to ORS of any  $p^{th}$  hop,  $f_{h_a}^{(p)}$  is given as [7]

$$f_{h_a}^{(p)}(x) = \frac{A}{x} G_{1 \frac{1}{2}}^{2 \frac{1}{2}} \left( \frac{\alpha^{(p)}\beta^{(p)}x}{\lambda^{(p)} - 1} \middle| \frac{1 - \lambda^{(p)}}{\alpha^{(p)}, \beta^{(p)}} \right) \quad (2.7)$$

where  $\alpha^{(p)}$ ,  $\beta^{(p)}$  and  $\lambda^{(p)} = \alpha^{(p)} + 2$  are the large, medium and small scale scattering parameters,  $G_{p,q}^{m,n}(\cdot)$  represents the Meijer's G-function. The expression for  $A$  is given as

$$A = \frac{1}{\Gamma(\alpha^{(p)})\Gamma(\beta^{(p)})\Gamma(\lambda^{(p)})} \quad (2.8)$$

#### 2.1.2 Pointing error fading model

The misalignment between the transmitter beam and receiver aperture will lead to pointing errors. These misalignments happen due to vibrations in the building, thermal expansion etc. The fraction of power received at the photodetector is given as [5]

$$h_{pe}^{(p)} = A_0 \exp \left( \frac{-2(r^{(p)})^2}{w_{zeq}^2} \right) \quad (2.9)$$

where  $r^{(p)}$  is the radial displacement,  $A_0 = erf^2(d)$  is the power received when  $r^{(p)} = 0$ ,  $erf(\cdot)$  is the error function,  $d = \sqrt{\frac{\pi}{2}} \frac{a_z}{w_z}$ ,  $a_z$  is aperture radius of the receiving lens,  $w_z$  is the incoming optical beamwidth and the equivalent beamwidth  $w_{zeq}$  is given as  $w_{zeq}^2 = w_z^2 \frac{\sqrt{\pi} erf(d)}{2d exp(-d^2)}$ . The radial displacement of the incoming beam away from the center of the receiver aperture is modelled using the Rayleigh distribution. So, the PDF of radial displacement can be written as

$$f_r^{(p)}(r) = \frac{r}{(\sigma^{(p)})^2} \exp \left( \frac{-r^2}{2(\sigma^{(p)})^2} \right) \quad (2.10)$$

where  $\sigma^{(p)}$  is the jitter standard deviation. By using the above equations the PDF of pointing error can be written as

$$f_{h_{pe}}^{(p)}(x) = \frac{(g^{(p)})^2}{A_0} \left( \frac{x}{A_0} \right)^{(g^{(p)})^2 - 1} \quad (2.11)$$

where  $0 < x < A_0$  and pointing error coefficient  $g^{(p)} = \frac{w_{zeq}}{2\sigma^{(p)}}$ .

### 2.1.3 Fog fading model

The channel state of fog  $h_f^{(p)}$ , is modeled with the help of Beer-Lambert's law and can be written as  $h_f^{(p)} = e^{-\tau L^{(p)}/4.343}$ , where  $\tau$  is the attenuation coefficient in dB/km which is gamma distributed and  $L^{(p)}$  is the link distance in km. The PDF of fog is given as [5]

$$f_{h_f}^{(p)}(x) = \frac{(v^{(p)})^{k^{(p)}}}{\Gamma(k^{(p)})} \left[ \ln \left( \frac{1}{x} \right) \right]^{k^{(p)} - 1} x^{v^{(p)} - 1} \quad (2.12)$$

where  $0 < x \leq 1$ ,  $v^{(p)} = \frac{4.343}{L^{(p)}\psi^{(p)}}$ ,  $\psi^{(p)}$  is size parameter and  $k^{(p)}$  is shape parameter.

## 2.2 Combined channel model

The channel coefficient from the transmitter to ORS,  $h_1^{(p)}$  is given as  $h_1^{(p)} = h_{a_1}^{(p)} h_{pe_1}^{(p)} h_{f_1}^{(p)}$  and from ORS to Rx is given as  $h_2^{(p)} = h_{a_2}^{(p)} h_{pe_2}^{(p)} h_{f_2}^{(p)}$ . The overall channel coefficient for any  $p^{th}$  hop is given as  $Z_p = h_1^{(p)} h_2^{(p)}$ .

### 2.2.1 Gamma-Gamma distribution

The combined channel PDF of the  $p^{th}$  hop for Gamma-Gamma distribution is given as [5]

$$f_{Z_p}(x) = \frac{1}{x} \left( \zeta_1^{(p)} \zeta_2^{(p)} \right)^{-1} \left( \chi_1^{(p)} \chi_2^{(p)} \right) \left( (v_1^{(p)})^{k_1^{(p)}} (v_2^{(p)})^{k_2^{(p)}} \right) G_{2+k_1^{(p)}+k_2^{(p)} \atop 6+k_1^{(p)}+k_2^{(p)}}^{6+k_1^{(p)}+k_2^{(p)} \atop 0} \left( \left( (\zeta_1^{(p)} \zeta_2^{(p)}) x \right) \left| \begin{matrix} \Delta_1 \\ \Delta_2 \end{matrix} \right. \right) \quad (2.13)$$

where  $\chi_i^{(p)} = \frac{\alpha_i^{(p)} \beta_i^{(p)} (g_i^{(p)})^2}{A_0 \Gamma(\alpha_i^{(p)}) \Gamma(\beta_i^{(p)})}$ ,  $\zeta_i^{(p)} = \frac{\alpha_i^{(p)} \beta_i^{(p)}}{A_0}$  and other notations are given in Table 2.1.

The instantaneous and average electrical SNR of any  $p^{th}$  hop is given as

$$\gamma^{(p)} = \frac{(P_F \eta Z_p)^2}{\sigma_{op}^2} \quad (2.14)$$

and

$$\overline{\gamma^{(p)}} = \frac{(P_F \eta)^2}{\sigma_{o_p}^2} (\mathbb{E}[Z_p])^2 \quad (2.15)$$

where  $P_F$  is the optical power of the transmitted signal,  $\eta$  is responsivity and  $\sigma_{o_p}^2$  is the AWGN variance. The expression for  $\mathbb{E}[Z_p]$  is given as

$$\mathbb{E}[Z_p] = A_0^2 \prod_{i=1}^2 \left( \frac{(g_i^{(p)})^2}{1 + (g_i^{(p)})^2} \right) \left( \frac{v_i^{(p)}}{1 + v_i^{(p)}} \right)^{k_i^{(p)}} \quad (2.16)$$

Let's assume that  $\mathbb{E}[Z_p] = B$ . From Eq. (2.14) and Eq. (2.15), the relation between instantaneous and average electrical SNR is given as  $\gamma^{(p)} = \frac{\overline{\gamma^{(p)}} Z_p^2}{B^2}$ . By applying the transformation of random variables, the PDF of  $f_{\gamma^{(p)}}(\gamma)$  is given as

$$f_{\gamma^{(p)}}(\gamma) = \frac{1}{2\gamma} \left( \zeta_1^{(p)} \zeta_2^{(p)} \right)^{-1} \left( \chi_1^{(p)} \chi_2^{(p)} \right) \left( (v_1^{(p)})^{k_1^{(p)}} (v_2^{(p)})^{k_2^{(p)}} \right) G_{2+k_1^{(p)}+k_2^{(p)} \atop 2+k_1^{(p)}+k_2^{(p)} \atop 6+k_1^{(p)}+k_2^{(p)}}^{\begin{matrix} 6+k_1^{(p)}+k_2^{(p)} \\ 0 \end{matrix}} \left( \left( (\zeta_1^{(p)} \zeta_2^{(p)}) \sqrt{\frac{\gamma B^2}{\gamma^{(p)}}} \right) \left| \begin{matrix} \Delta_1 \\ \Delta_2 \end{matrix} \right. \right) \quad (2.17)$$

### 2.2.2 Málaga Distribution

The combined channel PDF from transmitter to ORS for any  $p^{th}$  hop  $h_i^{(p)}$ , for Málaga distribution can be computed by solving the following integral

$$f_{h_i^{(p)}}(x) = \int_x^\infty f_{h_{ape_i}^{(p)}}(\rho) f_{h_f^{(p)}}\left(\frac{x}{\rho}\right) \frac{1}{\rho} d\rho \quad (2.18)$$

where  $h_{ape_i}^{(p)} = h_{a_i}^{(p)} h_{pe_i}^{(p)}$  and using Eqs. (2.4) and (2.11) the PDF of  $h_{ape_i}^{(p)}$  is given as [6]

$$f_{h_{ape_i}^{(p)}}(x) = \chi_i^{(p)} \sum_{d_i^{(p)}=1}^{\beta_i^{(p)}} b_d G_{1 \atop 1 \atop 3}^{\begin{matrix} \beta_i^{(p)} \\ 0 \end{matrix}} \left( \zeta_i^{(p)} x \left| \begin{matrix} (g_i^{(p)})^2 \\ (g_i^{(p)})^2 - 1, \alpha_i^{(p)} - 1, d_i^{(p)} - 1 \end{matrix} \right. \right) \quad (2.19)$$

where  $b_d = a_d \frac{y_i^{(p)} \beta_i^{(p)} + \Omega_i^{(p)}}{(\alpha_i^{(p)} \beta_i^{(p)}) \frac{\alpha_i^{(p)} + d_i^{(p)}}{2}}$ ,  $\chi_i^{(p)} = \frac{A_{M_i}^{(p)} \alpha_i^{(p)} \beta_i^{(p)} (g_i^{(p)})^2}{2A_0 (y_i^{(p)} \beta_i^{(p)} + \Omega_i^{(p)})}$  and  $\zeta_i^{(p)} = \frac{\alpha_i^{(p)} \beta_i^{(p)}}{A_0 (y_i^{(p)} \beta_i^{(p)} + \Omega_i^{(p)})}$ . Using Eqs. (2.19), (2.12) and (2.18) and [9, Eq. (07.34.02.001.01)], we get

$$f_{h_i^{(p)}}(x) = \frac{\chi_i^{(p)} (v_i^{(p)})^{k_i^{(p)}}}{\Gamma(k_i^{(p)})} x^{v_i^{(p)}-1} \sum_{d_i^{(p)}=1}^{\beta_i^{(p)}} b_d \frac{1}{2\pi \mathcal{J}} \int_{\mathcal{L}} \frac{\Gamma((g_i^{(p)})^2 - 1 - s)}{\Gamma((g_i^{(p)})^2 - s)} \Gamma(\alpha_i^{(p)} - 1 - s) \Gamma(d_i^{(p)} - 1 - s) \int_x^\infty \rho^{s-v_i^{(p)}} \left( \ln \frac{\rho}{x} \right)^{k_i^{(p)}-1} d\rho (\zeta_i^{(p)})^s ds \quad (2.20)$$

where  $\mathcal{J} = \sqrt{-1}$ . By solving the inner integral of Eq. (2.20) using [8, Eq. (3.326.2)] and applying the definition of Meijer's G-function, the PDF of  $h_{i(p)}$  is given as

$$f_{h_{i(p)}}(x) = \chi_i^{(p)}(v_i^{(p)})^{k_i^{(p)}} \sum_{d_i^{(p)}=1}^{\beta_i^{(p)}} b_d G_{1+k_i^{(p)} \atop 3+k_i^{(p)}}^{3+k_i^{(p)} \atop 0} \times \left( \zeta_i^{(p)} x \left| \begin{matrix} (g_i^{(p)})^2, \{v_i^{(p)}\}_1^{k_i^{(p)}} \\ (g_i^{(p)})^2 - 1, \alpha_i^{(p)} - 1, d_i^{(p)} - 1, \{v_i^{(p)} - 1\}_1^{k_i^{(p)}} \end{matrix} \right. \right) \quad (2.21)$$

The PDF of the overall channel coefficient,  $Z_p$  for the Málaga distribution can be derived using the following integral

$$f_{Z_p}(x) = \int_0^\infty f_{h_1(p)}(\rho) f_{h_2(p)}\left(\frac{x}{\rho}\right) \frac{1}{\rho} d\rho \quad (2.22)$$

Substituting Eq. (2.21) in (2.22) and applying [9, Eq. (07.34.21.0011.01)], the PDF of  $Z_p$  is given as

$$f_{Z_p}(x) = \frac{1}{x} \left( \zeta_1^{(p)} \zeta_2^{(p)} \right)^{-1} \left( \chi_1^{(p)} \chi_2^{(p)} \right) \left( (v_1^{(p)})^{k_1^{(p)}} (v_2^{(p)})^{k_2^{(p)}} \right) \sum_{d_1^{(p)}=1}^{\beta_1^{(p)}} \sum_{d_2^{(p)}=1}^{\beta_2^{(p)}} b_{d_1} b_{d_2} G_{2+k_1^{(p)}+k_2^{(p)} \atop 6+k_1^{(p)}+k_2^{(p)}}^{6+k_1^{(p)}+k_2^{(p)} \atop 0} \left( \left( (\zeta_1^{(p)} \zeta_2^{(p)}) x \right) \left| \begin{matrix} \Delta_1 \\ \Delta_3 \end{matrix} \right. \right) \quad (2.23)$$

The expression for  $\mathbb{E}[Z_p]$  is given as

$$\mathbb{E}[Z_p] = A_0^2 \prod_{i=1}^2 \left( y_i^{(p)} + \Omega_i'^{(p)} \right) \left( \frac{(g_i^{(p)})^2}{1 + (g_i^{(p)})^2} \right) \left( \frac{v_i^{(p)}}{1 + v_i^{(p)}} \right)^{k_i^{(p)}} \quad (2.24)$$

Let's assume that  $\mathbb{E}[Z_p] = B$ . By using the relation between instantaneous and average electrical SNR and applying the transformation of random variables, the PDF of  $f_{\gamma(p)}(\gamma)$  is given as

$$f_{\gamma(p)}(\gamma) = \frac{1}{2\gamma} \left( \zeta_1^{(p)} \zeta_2^{(p)} \right)^{-1} \left( \chi_1^{(p)} \chi_2^{(p)} \right) \left( (v_1^{(p)})^{k_1^{(p)}} (v_2^{(p)})^{k_2^{(p)}} \right) \sum_{d_1^{(p)}=1}^{\beta_1^{(p)}} \sum_{d_2^{(p)}=1}^{\beta_2^{(p)}} b_{d_1} b_{d_2} G_{2+k_1^{(p)}+k_2^{(p)} \atop 6+k_1^{(p)}+k_2^{(p)}}^{6+k_1^{(p)}+k_2^{(p)} \atop 0} \left( \left( (\zeta_1^{(p)} \zeta_2^{(p)}) \sqrt{\frac{\gamma B^2}{\gamma^{(p)}}} \right) \left| \begin{matrix} \Delta_1 \\ \Delta_3 \end{matrix} \right. \right) \quad (2.25)$$

### 2.2.3 IGGG Distribution

Using Eqs. (2.7) and (2.11) the PDF of  $h_{ape_i}^{(p)}$  is given as

$$f_{h_{ape_i}^{(p)}}(x) = \chi_i^{(p)} G_{\frac{3}{2} \frac{1}{3}} \left( \zeta_i^{(p)} x \left| \begin{matrix} -\lambda_i^{(p)}, (g_i^{(p)})^2 \\ (g_i^{(p)})^2 - 1, \alpha_i^{(p)} - 1, \beta_i^{(p)} - 1 \end{matrix} \right. \right) \quad (2.26)$$

where  $\chi_i^{(p)} = \frac{A_i^{(p)} \alpha_i^{(p)} \beta_i^{(p)} (g_i^{(p)})^2}{A_0(\lambda_i^{(p)} - 1)}$  and  $\zeta_i^{(p)} = \frac{\alpha_i^{(p)} \beta_i^{(p)}}{A_0(\lambda_i^{(p)} - 1)}$ . Using Eqs. (2.26), (2.12) and (2.18) and [9, Eq. 07.34.02.001.01], we get

$$f_{h_i^{(p)}}(x) = \frac{\chi_i^{(p)} (v_i^{(p)})^{k_i^{(p)}}}{\Gamma(k_i^{(p)})} x^{v_i^{(p)} - 1} \frac{1}{2\pi \mathcal{J}} \int_{\mathcal{L}} \frac{\Gamma((g_i^{(p)})^2 - 1 - s) \Gamma(1 + \lambda_i^{(p)} + s)}{\Gamma((g_i^{(p)})^2 - s)} \Gamma(\alpha_i^{(p)} - 1 - s) \Gamma(\beta_i^{(p)} - 1 - s) \int_x^\infty \rho^{s - v_i^{(p)}} \left( \ln \frac{\rho}{x} \right)^{k_i^{(p)} - 1} d\rho (\zeta_i^{(p)})^s ds \quad (2.27)$$

where  $\mathcal{J} = \sqrt{-1}$ . By solving the inner integral of Eq. (2.27) using [8, Eq. 3.326.2] and applying the definition of Meijer's G-function, the PDF of  $h_{i(p)}$  is given as

$$f_{h_i^{(p)}}(x) = \chi_i^{(p)} (v_i^{(p)})^{k_i^{(p)}} G_{\frac{3+k_i^{(p)}}{2+k_i^{(p)}} \frac{1}{3+k_i^{(p)}}} \left( \zeta_i^{(p)} x \left| \begin{matrix} -\lambda_i^{(p)}, (g_i^{(p)})^2, \{v_i^{(p)}\}_1^{k_i^{(p)}} \\ (g_i^{(p)})^2 - 1, \alpha_i^{(p)} - 1, \beta_i^{(p)} - 1, \{v_i^{(p)} - 1\}_1^{k_i^{(p)}} \end{matrix} \right. \right) \quad (2.28)$$

Substituting Eq. (2.28) in (2.22) and applying [9, Eq. 07.34.21.0011.01], the PDF of  $Z_p$  is given as

$$f_{Z_p}(x) = \frac{1}{x} \left( \zeta_1^{(p)} \zeta_2^{(p)} \right)^{-1} \left( \chi_1^{(p)} \chi_2^{(p)} \right) \left( (v_1^{(p)})^{k_1^{(p)}} (v_2^{(p)})^{k_2^{(p)}} \right) G_{\frac{6+k_1^{(p)}+k_2^{(p)}}{4+k_1^{(p)}+k_2^{(p)}} \frac{2}{6+k_1^{(p)}+k_2^{(p)}}} \left( \left( (\zeta_1^{(p)} \zeta_2^{(p)}) x \right) \left| \begin{matrix} \Delta_4 \\ \Delta_2 \end{matrix} \right. \right) \quad (2.29)$$

The expression for  $\mathbb{E}[Z_p]$  is given as

$$\mathbb{E}[Z_p] = A_0^2 \prod_{i=1}^2 \left( \frac{(g_i^{(p)})^2}{1 + (g_i^{(p)})^2} \right) \left( \frac{v_i^{(p)}}{1 + v_i^{(p)}} \right)^{k_i^{(p)}} \quad (2.30)$$

Let's assume that  $\mathbb{E}[Z_p] = B$ . By using the relation between instantaneous and average electrical SNR and applying the transformation of random variables, the PDF of  $f_{\gamma^{(p)}}(\gamma)$

is given as

$$f_{\gamma^{(p)}}(\gamma) = \frac{1}{2\gamma} \left( \zeta_1^{(p)} \zeta_2^{(p)} \right)^{-1} \left( \chi_1^{(p)} \chi_2^{(p)} \right) \left( (v_1^{(p)})^{k_1^{(p)}} (v_2^{(p)})^{k_2^{(p)}} \right) \\ G_{4+k_1^{(p)}+k_2^{(p)} \quad 6+k_1^{(p)}+k_2^{(p)}}^{6+k_1^{(p)}+k_2^{(p)} \quad 2} \left( \left( \zeta_1^{(p)} \zeta_2^{(p)} \right) \sqrt{\frac{\gamma B^2}{\gamma^{(p)}}} \right) \left| \frac{\Delta_4}{\Delta_2} \right| \quad (2.31)$$

Table 2.1: List of notations

|   |
|---|
| $\Delta_1 = 1 + (g_1^{(p)})^2, 1 + (g_2^{(p)})^2, \{1 + v_1^{(p)}\}_1^{k_1^{(p)}}, \{1 + v_2^{(p)}\}_1^{k_2^{(p)}}$   |
| $\Delta_2 = (g_1^{(p)})^2, (g_2^{(p)})^2, \alpha_1^{(p)}, \alpha_2^{(p)}, \beta_1^{(p)}, \beta_2^{(p)}, \{v_1^{(p)}\}_1^{k_1^{(p)}}, \{v_2^{(p)}\}_1^{k_2^{(p)}}$ |
| $\Delta_3 = (g_1^{(p)})^2, (g_2^{(p)})^2, \alpha_1^{(p)}, \alpha_2^{(p)}, d_1^{(p)}, d_2^{(p)}, \{v_1^{(p)}\}_1^{k_1^{(p)}}, \{v_2^{(p)}\}_1^{k_2^{(p)}}$         |
| $\Delta_4 = 1 - \lambda_1^{(p)}, 1 - \lambda_2^{(p)}, 1 + (g_1^{(p)})^2, 1 + (g_2^{(p)})^2, \{1 + v_1^{(p)}\}_1^{k_1^{(p)}}, \{1 + v_2^{(p)}\}_1^{k_2^{(p)}}$     |
| $\{a\}_1^l = \underbrace{\{a, a, \dots, a, a\}}_{l \text{ times}}$  |

## Chapter 3

# Ergodic Capacity analysis of the system using Gamma-Gamma distribution

The ergodic capacity for the  $p^{th}$  hop of the proposed system model for Gamma-Gamma distribution can be derived using the following equation

$$C^{(p)} = \mathbb{E}[\log_2(1 + s_r \gamma)] \quad (3.1)$$

where  $s_r = \begin{cases} s_r = 1(HD) \\ s_r = \frac{e}{2\pi}(IM/DD) \end{cases}$ . The min-cut max-flow theorem states that a system's overall capacity cannot exceed the capacity of an individual hop, indicating an upper bound for capacity. Therefore, the upper bound for the capacity is given as [10]

$$C_{DF} = \min(C^{(1)}, C^{(2)}, \dots, C^{(N)}) \quad (3.2)$$

The capacity of the  $p^{th}$  hop is derived by solving the integral

$$C^{(p)} = \int_0^\infty \log_2(1 + s_r \gamma) f_{\gamma^{(p)}}(\gamma) d\gamma \quad (3.3)$$

By substituting Eq. (2.17) in (3.3) and using [9, Eq. 07.34.030456.01], the integral can be written as

$$C^{(p)} = \frac{\left(\zeta_1^{(p)} \zeta_2^{(p)}\right)^{-1} \left(\chi_1^{(p)} \chi_2^{(p)}\right) \left((v_1^{(p)})_{k_1^{(p)}} (v_2^{(p)})_{k_2^{(p)}}\right)}{2 \ln 2} \int_0^\infty \frac{1}{\gamma} G_{\frac{1}{2} \frac{2}{2}} \left( s_r \gamma \left| \begin{matrix} 1, 1 \\ 1, 0 \end{matrix} \right. \right) G_{\frac{6+k_1^{(p)}+k_2^{(p)}}{2+k_1^{(p)}+k_2^{(p)}} \frac{0}{6+k_1^{(p)}+k_2^{(p)}}} \left( \left( \left( \zeta_1^{(p)} \zeta_2^{(p)} \right) \sqrt{\frac{\gamma B^2}{\gamma^{(p)}}} \right) \left| \begin{matrix} \Delta_1 \\ \Delta_2 \end{matrix} \right. \right) d\gamma \quad (3.4)$$



By using [9, Eq. 07.34.21.0013.01], the expression for ergodic capacity of  $p^{th}$  hop is given by

$$C^{(p)} = \frac{2^{\alpha_1^{(p)} + \alpha_2^{(p)} + \beta_1^{(p)} + \beta_2^{(p)} - k_1^{(p)} - k_2^{(p)} - 6}}{\pi^2 \ln 2} \left( \zeta_1^{(p)} \zeta_2^{(p)} \right)^{-1} \left( \chi_1^{(p)} \chi_2^{(p)} \right) \left( (v_1^{(p)})^{k_1^{(p)}} (v_2^{(p)})^{k_2^{(p)}} \right) \\ G_{6+2k_1^{(p)}+2k_2^{(p)}}^{14+2k_1^{(p)}+2k_2^{(p)}} \frac{1}{14+2k_1^{(p)}+2k_2^{(p)}} \left( \frac{(\zeta_1^{(p)} \zeta_2^{(p)})^2 B^2}{256 s_r \gamma^{(p)}} \left| \frac{\Delta_5}{\Delta_6} \right| \right) \quad (3.5)$$

where the notations used in the above equations is mentioned in Table 3.1. The overall ergodic capacity of the system can be calculated using Eq. (3.2).

Table 3.1: List of notations for ergodic capacity

|  |
|--|
| $\Delta_5 = 0, 1, \frac{1+(g_1^{(p)})^2}{2}, \frac{2+(g_1^{(p)})^2}{2}, \frac{1+(g_2^{(p)})^2}{2}, \frac{2+(g_2^{(p)})^2}{2}, \left\{ \frac{1+v_1^{(p)}}{2} \right\}_1^{k_1^{(p)}}, \left\{ \frac{2+v_1^{(p)}}{2} \right\}_1^{k_1^{(p)}}, \left\{ \frac{1+v_2^{(p)}}{2} \right\}_1^{k_2^{(p)}}, \left\{ \frac{2+v_2^{(p)}}{2} \right\}_1^{k_2^{(p)}}$  |
| $\Delta_6 = \frac{(g_1^{(p)})^2}{2}, \frac{1+(g_1^{(p)})^2}{2}, \frac{(g_2^{(p)})^2}{2}, \frac{1+(g_2^{(p)})^2}{2}, \frac{\alpha_1^{(p)}}{2}, \frac{1+\alpha_1^{(p)}}{2}, \frac{\alpha_2^{(p)}}{2}, \frac{1+\alpha_2^{(p)}}{2}, \frac{\beta_1^{(p)}}{2}, \frac{1+\beta_1^{(p)}}{2}, \frac{\beta_2^{(p)}}{2}, \frac{1+\beta_2^{(p)}}{2},$<br>$\left\{ \frac{v_1^{(p)}}{2} \right\}_1^{k_1^{(p)}}, \left\{ \frac{1+v_1^{(p)}}{2} \right\}_1^{k_1^{(p)}}, \left\{ \frac{v_2^{(p)}}{2} \right\}_1^{k_2^{(p)}}, \left\{ \frac{1+v_2^{(p)}}{2} \right\}_1^{k_2^{(p)}}, 0, 0$ |
| $\Delta_7 = \frac{(g_1^{(p)})^2}{2}, \frac{1+(g_1^{(p)})^2}{2}, \frac{(g_2^{(p)})^2}{2}, \frac{1+(g_2^{(p)})^2}{2}, \frac{\alpha_1^{(p)}}{2}, \frac{1+\alpha_1^{(p)}}{2}, \frac{\alpha_2^{(p)}}{2}, \frac{1+\alpha_2^{(p)}}{2}, \frac{d_1^{(p)}}{2}, \frac{1+d_1^{(p)}}{2}, \frac{d_2^{(p)}}{2}, \frac{1+d_2^{(p)}}{2},$<br>$\left\{ \frac{v_1^{(p)}}{2} \right\}_1^{k_1^{(p)}}, \left\{ \frac{1+v_1^{(p)}}{2} \right\}_1^{k_1^{(p)}}, \left\{ \frac{v_2^{(p)}}{2} \right\}_1^{k_2^{(p)}}, \left\{ \frac{1+v_2^{(p)}}{2} \right\}_1^{k_2^{(p)}}, 0, 0$                 |
| $\Delta_8 = \frac{1-\lambda_1^{(p)}}{2}, \frac{2-\lambda_1^{(p)}}{2}, \frac{1-\lambda_2^{(p)}}{2}, \frac{2-\lambda_2^{(p)}}{2}, 0, 1, \frac{1+(g_1^{(p)})^2}{2}, \frac{2+(g_1^{(p)})^2}{2}, \frac{1+(g_2^{(p)})^2}{2}, \frac{2+(g_2^{(p)})^2}{2},$<br>$\left\{ \frac{1+v_1^{(p)}}{2} \right\}_1^{k_1^{(p)}}, \left\{ \frac{2+v_1^{(p)}}{2} \right\}_1^{k_1^{(p)}}, \left\{ \frac{1+v_2^{(p)}}{2} \right\}_1^{k_2^{(p)}}, \left\{ \frac{2+v_2^{(p)}}{2} \right\}_1^{k_2^{(p)}}$   |

## Chapter 4

# Ergodic Capacity analysis of the system using Málaga distribution

The ergodic capacity for the  $p^{th}$  hop of the proposed system model for Málaga distribution can be derived using the following equation

$$C^{(p)} = \mathbb{E}[\log_2(1 + s_r \gamma)] \quad (4.1)$$

where  $s_r = \begin{cases} s_r = 1(HD) \\ s_r = \frac{e}{2\pi}(IM/DD) \end{cases}$ . The min-cut max-flow theorem states that a system's overall capacity cannot exceed the capacity of an individual hop, indicating an upper bound for capacity. Therefore, the upper bound for the capacity is given as [10]

$$C_{DF} = \min(C^{(1)}, C^{(2)}, \dots, C^{(N)}) \quad (4.2)$$

The capacity of the  $p^{th}$  hop is derived by solving the integral

$$C^{(p)} = \int_0^\infty \log_2(1 + s_r \gamma) f_{\gamma^{(p)}}(\gamma) d\gamma \quad (4.3)$$

By substituting Eq. (2.25) in (4.3) and using [9, Eq. 07.34.030456.01], the integral can be written as

$$C^{(p)} = \frac{\left(\zeta_1^{(p)} \zeta_2^{(p)}\right)^{-1} \left(\chi_1^{(p)} \chi_2^{(p)}\right) \left((v_1^{(p)})^{k_1^{(p)}} (v_2^{(p)})^{k_2^{(p)}}\right)}{2 \ln 2} \sum_{d_1^{(p)}=1}^{\beta_1^{(p)}} \sum_{d_2^{(p)}=1}^{\beta_2^{(p)}} b_{d_1} b_{d_2} \int_0^\infty \frac{1}{\gamma} G_{\frac{1}{2} \frac{1}{2}}^{\frac{1}{2} \frac{2}{2}} \left( s_r \gamma \left| \begin{matrix} 1, 1 \\ 1, 0 \end{matrix} \right. \right) G_{\frac{6+k_1^{(p)}+k_2^{(p)}}{2+k_1^{(p)}+k_2^{(p)}} \frac{0}{6+k_1^{(p)}+k_2^{(p)}}} \left( \left( (\zeta_1^{(p)} \zeta_2^{(p)}) \sqrt{\frac{\gamma B^2}{\gamma^{(p)}}} \right) \left| \begin{matrix} \Delta_1 \\ \Delta_3 \end{matrix} \right. \right) d\gamma \quad (4.4)$$

By using [9, Eq. 07.34.21.0013.01], the expression for ergodic capacity of  $p^{th}$  hop is given by

$$C^{(p)} = \frac{\left(\zeta_1^{(p)} \zeta_2^{(p)}\right)^{-1} \left(\chi_1^{(p)} \chi_2^{(p)}\right) \left((v_1^{(p)})^{k_1^{(p)}} (v_2^{(p)})^{k_2^{(p)}}\right)}{\pi^2 l n 2} \sum_{d_1^{(p)}=1}^{\beta_1^{(p)}} \sum_{d_2^{(p)}=1}^{\beta_2^{(p)}} b_{d_1} b_{d_2} \quad (4.5)$$

$$2^{\alpha_1^{(p)} + \alpha_2^{(p)} + d_1^{(p)} + d_2^{(p)} - k_1^{(p)} - k_2^{(p)} - 6} G_{6+2k_1^{(p)}+2k_2^{(p)}}^{14+2k_1^{(p)}+2k_2^{(p)} \quad 1} \left( \frac{(\zeta_1^{(p)} \zeta_2^{(p)})^2 B^2}{256 s_r \gamma^{(p)}} \left| \begin{array}{c} \Delta_5 \\ \Delta_7 \end{array} \right. \right)$$

where the notations are mentioned in Table 3.1. The overall ergodic capacity of the system can be calculated using Eq. (4.2).

## Chapter 5

# Ergodic Capacity analysis of the system using IGGG distribution

The ergodic capacity for the  $p^{th}$  hop of the proposed system model for IGGG distribution can be derived using the following equation

$$C^{(p)} = \mathbb{E}[\log_2(1 + s_r \gamma)] \quad (5.1)$$

where  $s_r = \begin{cases} s_r = 1(HD) \\ s_r = \frac{e}{2\pi}(IM/DD) \end{cases}$ . The min-cut max-flow theorem states that a system's overall capacity cannot exceed the capacity of an individual hop, indicating an upper bound for capacity. Therefore, the upper bound for the capacity is given as [10]

$$C_{DF} = \min(C^{(1)}, C^{(2)}, \dots, C^{(N)}) \quad (5.2)$$

The capacity of the  $p^{th}$  hop is derived by solving the integral

$$C^{(p)} = \int_0^\infty \log_2(1 + s_r \gamma) f_{\gamma^{(p)}}(\gamma) d\gamma \quad (5.3)$$

By substituting Eq. (2.31) in (5.3) and using [9, Eq. 07.34.030456.01], the integral can be written as

$$C^{(p)} = \frac{\left(\zeta_1^{(p)} \zeta_2^{(p)}\right)^{-1} \left(\chi_1^{(p)} \chi_2^{(p)}\right) \left((v_1^{(p)})^{k_1^{(p)}} (v_2^{(p)})^{k_2^{(p)}}\right)}{2 \ln 2} \int_0^\infty \frac{1}{\gamma} G_{\frac{1}{2} \frac{2}{2}} \left( s_r \gamma \left| \begin{matrix} 1, 1 \\ 1, 0 \end{matrix} \right. \right) G_{\frac{6+k_1^{(p)}+k_2^{(p)}}{4+k_1^{(p)}+k_2^{(p)}} \frac{2}{6+k_1^{(p)}+k_2^{(p)}}} \left( \left( \zeta_1^{(p)} \zeta_2^{(p)} \right) \sqrt{\frac{\gamma B^2}{\gamma^{(p)}}} \left| \begin{matrix} \Delta_4 \\ \Delta_2 \end{matrix} \right. \right) d\gamma \quad (5.4)$$

By using [9, Eq. 07.34.21.0013.01], the expression for ergodic capacity of  $p^{th}$  hop is simplified into

$$C^{(p)} = \frac{2^{\alpha_1^{(p)} + \alpha_2^{(p)} + \beta_1^{(p)} + \beta_2^{(p)} + \lambda_1^{(p)} + \lambda_2^{(p)} - k_1^{(p)} - k_2^{(p)} - 8}}{\pi^3 \ln 2} \left( \zeta_1^{(p)} \zeta_2^{(p)} \right)^{-1} \left( \chi_1^{(p)} \chi_2^{(p)} \right) \left( (v_1^{(p)})^{k_1^{(p)}} (v_2^{(p)})^{k_2^{(p)}} \right) \\ G_{10+2k_1^{(p)}+2k_2^{(p)}}^{14+2k_1^{(p)}+2k_2^{(p)} \quad 5 \quad 14+2k_1^{(p)}+2k_2^{(p)}} \left( \frac{(\zeta_1^{(p)} \zeta_2^{(p)})^2 B^2}{16 s_r \gamma^{(p)}} \middle| \frac{\Delta_8}{\Delta_6} \right) \quad (5.5)$$

where the notations are mentioned in Table 3.1. And the overall ergodic capacity of the system can be calculated using Eq. (5.2).

# Chapter 6

## Numerical Results and Discussions

In this chapter, we have discussed the numerical and simulation results obtained from the closed-form expressions of ergodic capacity derived in Chapters 3, 4, and 5. The link distance between Tx to ORS and ORS to the detector in each hop is assumed to be the same, that is,  $L_1^{(p)} = L_2^{(p)}$ . To validate our analytical findings, we have performed Monte-Carlo simulations by generating 106 message symbols and independent channel coefficients. The values of the simulation parameters are given in Table 6.1, and Fig. 6.1 depicts the flowchart of Monte Carlo simulations.

Table 6.1: Simulation parameters

| Parameter                             | Values |
|---------------------------------------|--------|
| Shape parameter of fog, $k^{(p)}$     | 2      |
| Scale parameter of fog, $\psi^{(p)}$  | 13.12  |
| Pointing error coefficient, $g^{(p)}$ | 2.7    |
| Link distance (Tx to ORS), $L_1$      | 1000 m |
| Link distance (ORS to Rx), $L_2$      | 1000 m |
| No. of hops, $N$                      | 3      |

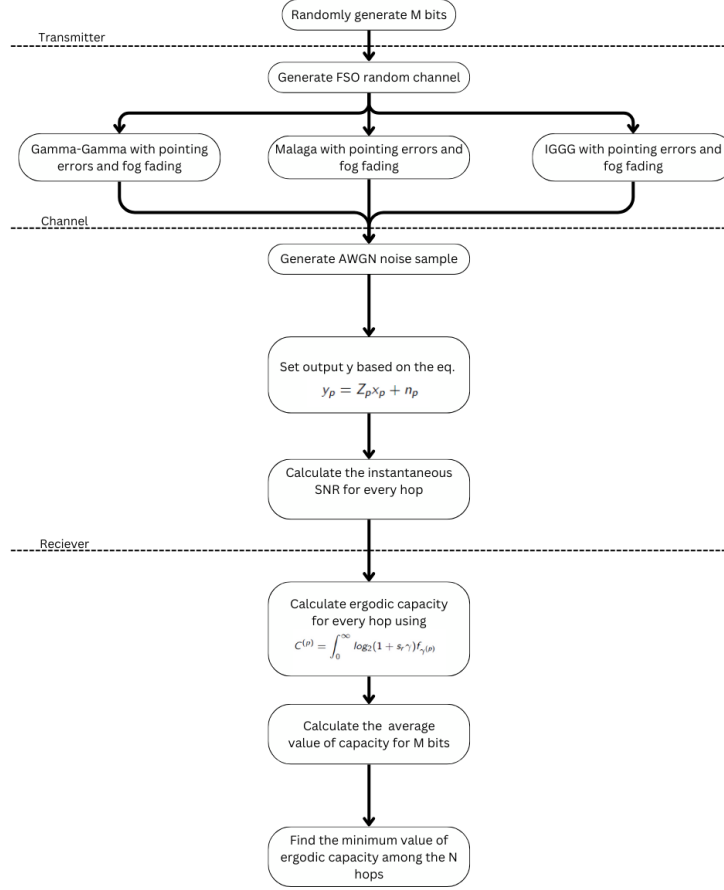


Figure 6.1: Flowchart of Monte-Carlo simulations for calculating ergodic capacity

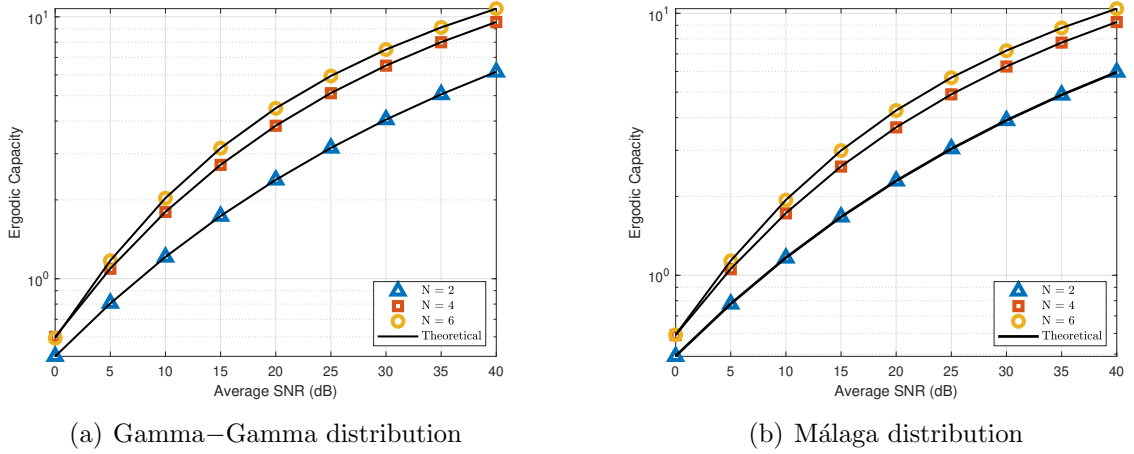


Figure 6.2: Ergodic capacity performance for N hops

Fig. 6.2 (a) and (b) depict the ergodic capacity plots of the proposed system model for Gamma–Gamma and Málaga distribution for N hops. The proposed system is able to meet the capacity requirement of the enhanced mobile broadband (eMBB) scenario of the 5G system (i.e., 6 bits/sec/Hz). To achieve a capacity of 6 bits/sec/Hz, the system with  $N = 6$  has an SNR gain of 3 dB and 14 dB compared to the system with  $N = 4$  and  $N = 2$ , respectively for Gamma–Gamma distribution. The system's performance

with Gamma–Gamma distribution is slightly better than with the Málaga distribution and almost equal with the IGGG distribution for the given simulation parameters. It is observed that with increasing  $N$  the performance of the system improves. As increasing  $N$  will reduce the link distance between subsequent hop, which reduces atmospheric turbulence severity (i.e. increase in the value of atmospheric turbulence parameter  $\alpha^{(p)}$  and  $\beta^{(p)}$ ).

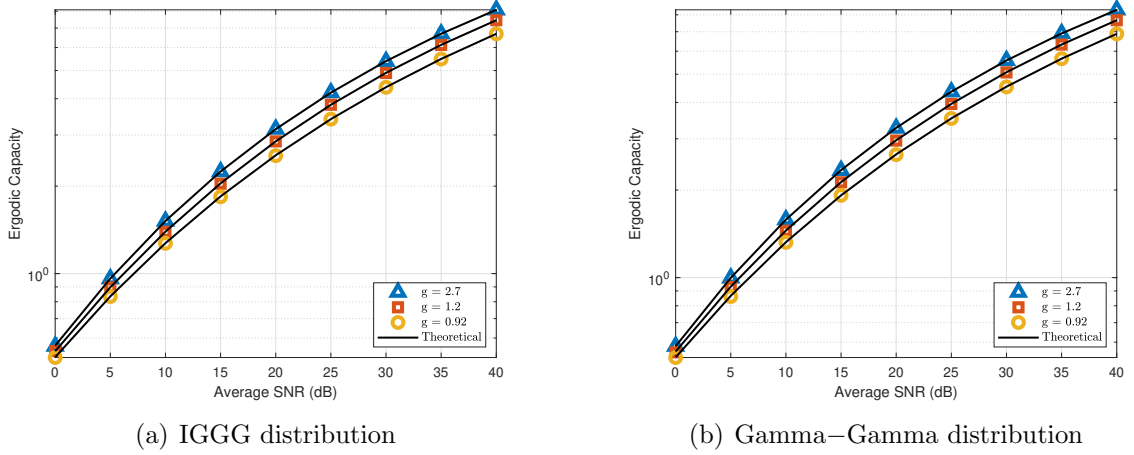


Figure 6.3: Ergodic capacity performance for different values of pointing error

Fig. 6.3 (a) and (b) depict the ergodic capacity plots for the proposed system model for IGGG and Gamma–Gamma distributions for different pointing error coefficient values. The system performance decreases as the value of the pointing error coefficient ( $g^{(p)}$ ) decreases because as the beam deviation increases, the pointing error coefficient value decreases. From the above plots, we can observe that,  $g^{(p)} = 2.7$  has an SNR gain of 2 dB and 4 dB as compared to the system with  $g^{(p)} = 1.2$  and  $g^{(p)} = 0.92$ , respectively, to obtain a capacity of 6 bits/sec/Hz.

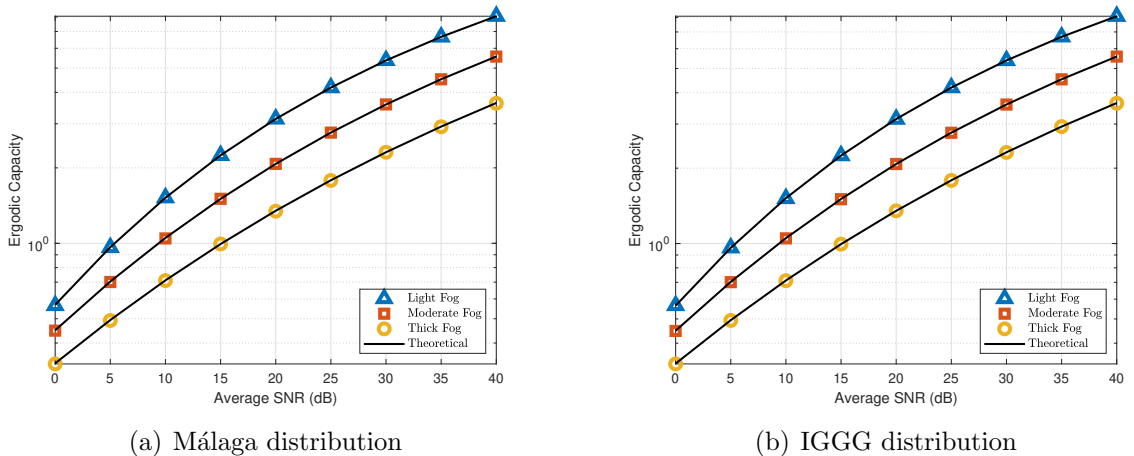
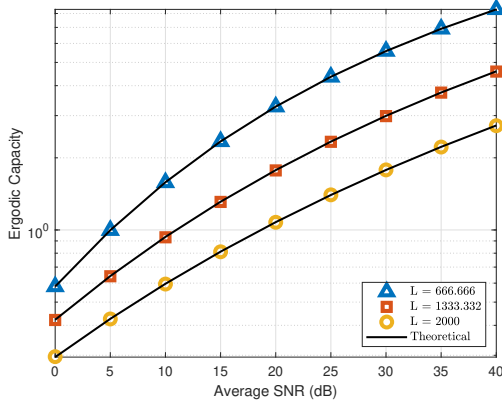


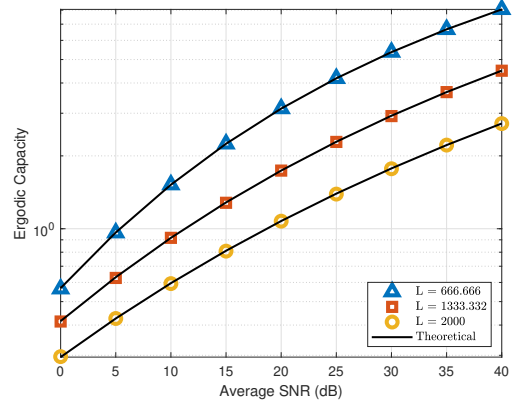
Figure 6.4: Ergodic capacity performance for different foggy weather conditions



In Fig. 6.4, we have obtained the ergodic capacity plot for different foggy weather conditions by keeping  $N = 3$  and in weak turbulence severity conditions. As the severity of the fog increases, the system performance decreases because, with the increase in severity of the fog, the size of the particles increases, which increases the absorption of the transmitted light. To achieve a capacity of 3 bits/sec/Hz, light fog condition has an SNR gain of 7 dB and 16 dB compared to the system with moderate and thick fog conditions.



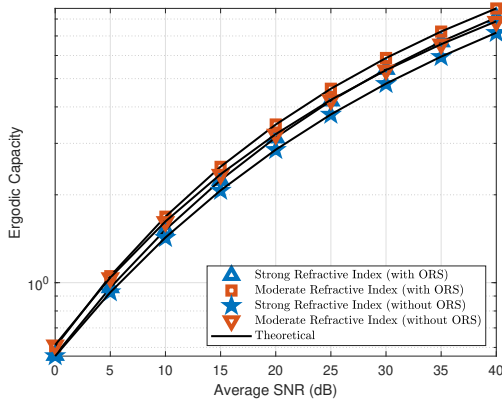
(a) Gamma–Gamma distribution



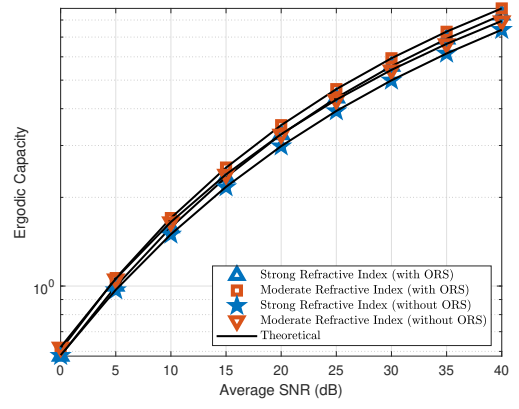
(b) Málaga distribution

Figure 6.5: Ergodic capacity performance for different link distances

Fig. 6.5 (a) and (b) depict the ergodic capacity vs. average SNR plot for different link distances between transmitter and receiver for Gamma–Gamma and Málaga distributions, respectively. As the link distance increases, the severity of atmospheric turbulence increases (i.e., the values of  $\alpha^{(p)}$  and  $\beta^{(p)}$  decrease), which decreases the value of the ergodic capacity. To achieve a capacity of 2 bits/sec/Hz, the system with the link distance  $L = 666.666$  has an SNR gain of almost 10 dB and 20 dB compared to a system with  $L = 1333.332$  and  $L = 2000$ , respectively.



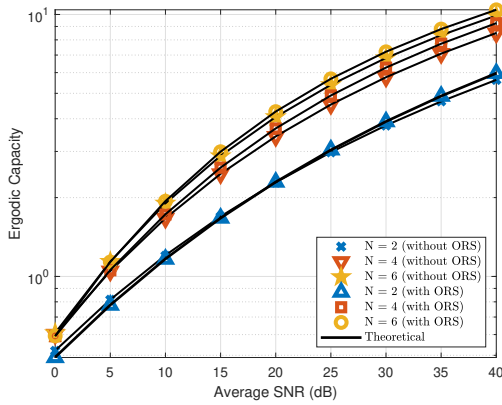
(a) IG-GG distribution



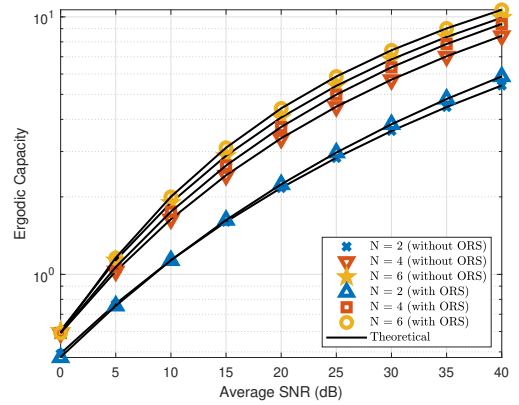
(b) Gamma-Gamma distribution

Figure 6.6: Ergodic capacity performance for different refractive index structure parameters

Fig. 6.6 shows the plot between the ergodic capacity and the average SNR for different refractive index structure parameters  $C_n^2$  for the IG-GG and Gamma-Gamma distributions. As the severity of atmospheric turbulence also increases, the value of the ergodic capacity decreases. To achieve a capacity of 5 bits/sec/Hz for strong refractive index conditions, the system with ORS has an SNR gain of 3 dB compared to the system without ORS. We can observe that at the higher values of average SNR, the system with ORS and moderate refractive index value ( $C_n^2 = 5 \times 10^{-14}$ ) outperforms the system without ORS and high refractive index value ( $C_n^2 = 2.3 \times 10^{-13}$ ).



(a) Málaga distribution



(b) IG-GG distribution

Figure 6.7: Comparison of ergodic capacity between systems with and without ORS

Fig. 6.7 depicts the comparison between the system with and without ORS for Málaga and IG-GG distributions. We can observe that the system with ORS has a better performance than the system without ORS. Even if there is a cascading effect due to ORS, the performance of the system improves, it is due to the decrease in the severity of all the

impediments affecting the channel (i.e., AT, PE, and fog). Also, the minimum capacity requirement eMBB usage scenario in a 5G system is achieved at an SNR of 25 dB with ORS, but without ORS it is achieved at an SNR of 28 dB for  $N = 6$ .

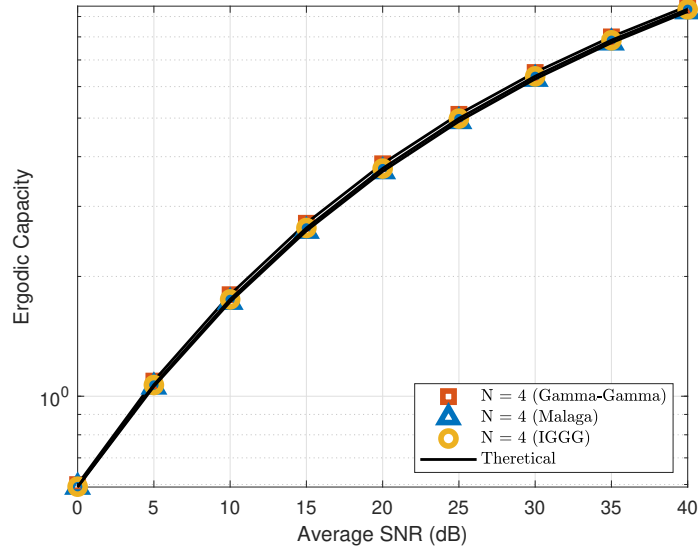


Figure 6.8: Comparison between Gamma–Gamma, Málaga and IGGG distributions

Fig. 6.8 depicts the comparison between Gamma–Gamma, Málaga and IGGG distributions for  $N = 4$ . When  $\lambda^{(p)} \rightarrow \infty$  (i.e.,  $\lambda^{(p)} \geq 13$ ), IGGG reduces to the Gamma–Gamma turbulence model, while all other parameters remain unchanged. Similarly for  $\rho^{(p)} = 1$ ,  $\Omega^{(p)} = 1$ , and  $y^{(p)} = 0$ , Málaga reduces to Gamma-Gamma model. As a special case, IGGG, and Málaga reduce to the Gamma-Gamma model.

# Chapter 7

## Conclusions and Future Work

### 7.1 Conclusion

This study examines the performance of a multihop ORS-assisted FSO communication system using DF relaying technique. It derives closed-form expressions for ergodic capacity for various atmospheric turbulence models, including Gamma–Gamma, Málaga, and IGGG distributions. Monte-Carlo simulations validate these expressions. The study finds that increasing pointing error severity and fog intensity decreases system performance due to attenuation, scattering, and absorption of optical signals. Comparing capacity performance of various models, the study finds that the Multihop ORS-assisted FSO system outperforms both Multihop FSO system without ORS and the single-hop ORS-assisted FSO systems.

### 7.2 Future scope of work

The scope for the future work can be summarized as follows:

- To obtain an asymptotic capacity expression for the given system model.
- We will extend our work to multi-hop  $N$  IRS element FSO communication system.
- The model discussed assumes perfect CSI conditions both at the ORS as well as at the receiver; imperfect CSI can be explored as a part of future work.
- For the ORS, perfect phase cancellation in order to maximize the SNR is assumed, as a part of the future work the non-ideal conditions for example non-unity ORS reflection coefficient and imperfect phase cancellation at ORS can be considered.

# References

- [1] E. Zedini, H. Soury, and M.-S. Alouini, “Dual-hop FSO transmission systems over gamma-gamma turbulence with pointing errors,” *IEEE Trans. Wireless Commun.* 16, 784–796 (2017).
- [2] E. Zedini, H. Soury, and M.-S. Alouini, “On the performance analysis of dual-hop mixed FSO/RF systems,” *IEEE Trans. Wireless Commun.* 15, 3679–3689 (2016).
- [3] T. A. Tsiftsis, H. G. Sandalidis, G. K. Karagiannidis, and N. C. Sagias, “Multihop free-space optical communications over strong turbulence channels,” *Proc. IEEE ICC.* 6, 2755–2759 (2006).
- [4] L. Yang, W. Guo, and I. S. Ansari, “Mixed dual-hop FSO-RF communication systems through reconfigurable intelligent surface,” *IEEE Commun. Lett.* 24, 1558–1562 (2020).
- [5] Smriti Uniyal, Narendra Viswakarma, and R. Swaminathan, “Multihop IRS-assisted free space optics communication with DF relaying: a performance analysis,” *J. Opt. Commun. Netw.* 62, 4716–4726 (2023).
- [6] D. Singh and R. Swaminathan, “Comprehensive performance analysis of hovering UAV-based FSO communication system,” *IEEE Photon. J.*, 14, 1–13, (2022).
- [7] P. Sharma, R. Swaminathan, and D. Singh, “Multi-hop UAV-based FSO system over doubly inverted gamma-gamma turbulence channel,” *IEEE Commun. Lett.*, 28, 2313–2317 (2024).
- [8] I. S. Gradshteyn and I. M. Ryzhik, *Table of Integrals, Series, and Products* (Academic, 2007).
- [9] The Wolfram functions site, “Hypergeometric functions,” [https:// functions.wolfram.com/HypergeometricFunctions/MeijerG](https://functions.wolfram.com/HypergeometricFunctions/MeijerG).

- [10] S. S. Ikki and S. Aissa, “Multihop wireless relaying systems in the presence of cochannel interferences: Performance analysis and design optimization,” *IEEE Trans. Veh. Technol.*, 61, 566–573 (2012).